Supporting Information

Anchoring and activation of catalytic sites on the clusters via intermolecular interactions

Feng Qian,[a,‡] Zhihang Zhao,[a,‡] Baoyu Huang,[b,‡] Zhixiang Xue,[a] Qinzhen Li,[a] Sha Yang,[a] Jinsong Chai[a,*] and Manzhou Zhu[a,*]

[a] School of Materials Science and Engineering and Centre for Atomic Engineering of Advanced Materials, Key Laboratory of Structure and Functional Regulation of Hybrid Materials of Ministry of Education, Anhui Province Key Laboratory of Chemistry for Inorganic/Organic Hybrid Functionalized Materials, Anhui University, Hefei, Anhui 230601, China.

*E-mail: chaijs@ahu.edu.cn; zmz@ahu.edu.cn

[b] Department Hunan Provincial Key Laboratory of Environmental Catalysis & Waste Recycling, College of Materials and Chemical Engineering, Hunan Institute of Engineering, 411104 Xiangtan, China

‡ These authors contributed equally to this work.

Experimental Procedures

Materials.

All reagents were commercially available and used without further purification. $HAuCl_4 \cdot 4H_2O$ (≥ 99.99%, metals basis) was purchased from China Nonferrous Metal Mining (Group) Co., Ltd. (Shenyang, China), and $CdCl_2 \cdot 2.5H_2O$ was purchased from Sigma-Aldrich (Shanghai, China). 1-Adamantanethiol (HS-Adm, ≥ 98%), 3,5-dimethyl-1-adamantanethiol (DM-SAdm, ≥ 95%), 4-Methoxythiophenol (4-MBT, ≥ 98%), Diphenyl-2-pyridylphosphine (PPh_2Py, ≥ 98%), (oxydi-2,1-phenylene)bis(diphenylphosphine) (OPDP, ≥ 98%), D-penicillamine (DPA, ≥ 98%), borane-tert-butylamine complex (≥ 95%) were purchased from Shanghai Macklin Biochemical Co., Ltd., and sodium borohydride ($NaBH_4$, ≥ 98%) were purchased from Shanghai Aladdin Bio-Chem Technology Co., Ltd. Solvents, including dichloromethane (DCM), methanol (MeOH), ethanol (EtOH), n-hexane (n-Hex), toluene (Tol), acetonitrile (MeCN) were HPLC grade. The ultrapure water (≥ 18.2 MΩ) used in this work was purified on a Millipore system (Millipore).

Measurements.

The TEM images were obtained by using a transmission electron microscope (JEM ARM-200F, JEOL). The crystal structures were analyzed by using an XRD (Smart Lab 9 kW, Japan) with Cu Kα radiation (λ = 0.15418 nm). UV-vis absorption spectra were recorded on an Agilent 8453 spectrophotometer. XPS measurements were performed on a thermal ESCALAB 250. ESI-MS were recorded using a Waters Xevo G2-XS mass spectrometer. The ORR electrochemical measurements were also performed on a CHI700E electrochemical workstation at room temperature.

Synthesis of $Au_{27}Cd_2(S\text{-}Adm)_{16}(PPh_2Py)Cl$.

First, 20 mg of $CdCl_2 \cdot 2.5H_2O$ and 400 μL $HAuCl_4 \cdot 4H_2O$ (0.2 g/mL in water) were dissolved in a mixed solvent (10 mL of EtOH and 10 mL of DCM). Then, 100 mg of HSAdm was added. After the color of the mixed solution turned light yellow, 5 mg of PPh_2Py was added. The mixed solution was stirred until it was transparent and colourless, and 120 mg of the borane-tert-butylamine complex was added. The mixture was stirred for 12 hours and washed with methanol several times. Dissolve the crude product with a small amount of DCM and add 5 mL TOL. Then, 60 mg of HS-Adm and 3 mg $CdCl_2 \cdot 2.5H_2O$ were added, and the reaction was stirred slowly at 60 °C for 12 hours. The insoluble precipitate in the crude product was removed by centrifugation, and the raw product was repeatedly washed with methanol. By TLC (DCM:n-Hex = 5:1, v:v), $Au_{27}Cd_2$ was extracted from the crude product. The pure $Au_{27}Cd_2$ was crystallized with chloroform/ethanol to obtain high-quality single crystals. The yield is 3.6% based on Au atoms.

Synthesis of $Au_{16}Cd_3(S\text{-}Adm)_9(PPh_2Py)_3Cl_3$.

First, 30 mg of $CdCl_2 \cdot 2.5H_2O$ and 400 μL $HAuCl_4 \cdot 4H_2O$ (0.2 g/mL in water) were dissolved in a mixed solvent (5 mL of EtOH and 15 mL of DCM). Then, 110 mg of HSAdm was added. After 15 minutes, 15 mg of PPh_2Py was added to the above solution. The mixed solution was stirred until it was transparent and colorless, and 120 mg of borane tert-butylamine complex was added. The mixture was stirred for 12 hours and washed with methanol several times. Second, the raw product was dissolved in 2 mL of DCM and 3 mL of Tol. Then, 60 mg of HS-Adm was added, and the reaction was stirred continuously and slowly at 60 °C for 12 hours.

The insoluble precipitate in the crude product was removed by centrifugation, and the raw product was repeatedly washed with methanol. By TLC (DCM:n-Hex = 5:1, v:v), $Au_{16}Cd_3$ was extracted from the crude product. The pure $Au_{16}Cd_3$ was crystallized with chloroform/ethanol to obtain high-quality single crystals. The yield is 5.2% based on Au atoms.

Synthesis of $Au_{19}Cd_3$(4-MBT)$_{18}$, $Au_{23}Cd_1(SAdm)_{14}$(OPDP)Cl, $Au_{24}Cd_1$(DM-SAdm)$_{13}$(DPPF)Cl and $Au_{30}Cd_1$(DM-SAdm)$_{18}$.

$Au_{19}Cd_3$(4-MBT)$_{18}$, $Au_{23}Cd_1(SAdm)_{14}$(OPDP)Cl, $Au_{24}Cd_1$(DM-SAdm)$_{13}$(DPPF)Cl and $Au_{30}Cd_1$(DM-SAdm)$_{18}$ was synthesized using the reported method.[1-2]

Synthesis of Au_{16}(S-Adm)$_{12}$, Au_{21}(S-Adm)$_{15}$ and Au_{24}(S-Adm)$_{16}$.

Au_{16}(S-Adm)$_{12}$, Au_{21}(S-Adm)$_{15}$ and Au_{24}(S-Adm)$_{16}$ was synthesized using the reported method.[3-5]

Preparation of electrocatalysts of nanoclusters.

50 mg of activated carbon was dispersed in 5 mL of dichloromethane, followed by the addition of 5 mg of clusters or complexes. The mixture was stirred for five hours, and the catalyst was obtained by centrifugation and dried in an oven for treatment. The nanoclusters are stable before and after electrocatalytic ORR.

Preparation of pyridine modified nanoclusters electrocatalysts.

50 mg of activated carbon was dispersed in 5 mL of dichloromethane, followed by the addition of 5 mg of clusters or complexes. 50 μL pyridine was added and stirred for 5 h, and the catalyst was centrifuged and dried in oven.

The Current-Time (IT) tests of nanocluster electrocatalysts and XPS characterization of $Au_{27}Cd_2$@C.

IT: Take 2 mg of the prepared electrocatalyst into an Erlenmeyer flask, add 1 mL of isopropyl alcohol and sonicate for 20 minutes. Then add 20 μL of Nafion and sonicate for another 10 minutes. Finally, take 20 μL of the solution and drop-coat it onto the carbon paper. Use 0.1 mol/L KOH as the electrolyte, and perform electrolysis at -1.4 V for 24 hours.

XPS: After the reaction, place the catalyst in the oven and dry it at 40 °C for 5 hours. Take 2 milligrams of the catalyst both before and after the reaction for XPS characterization.

Computational method and details.

The DFT calculations were performed with the Vienna Ab initio Simulation Package (VASP 5.4.1).[6] The projector augmented wave (PAW) method[7] with a generalized gradient approximation based on the Perdew–Burke–Erzerhof (PBE) exchange correlation functional is adopted.[8] The DFT-D3 method proposed by Grimme is applied to depict the van der Waals interactions.[9] The convergence criterion for the electronic structure iteration was set to be 10^{-4} eV, and that for geometry optimization was set to be 0.01 eV/Å on force. The plane–wave cutoff energy of 500 eV was used, and cells up to 30 Å in a vacuum region along directions a, b, and c avoid interactions between adjacent layers. All calculations in this work use the implicit Poissson-Boltzmann solvent model[10], and the dielectric constant is set as 80 for water.

Supplementary Notes.

The overall ORR could be expressed as $O_2 + 4H^+ + 4e^- \rightarrow 2H_2O$, it is also summarized as the following electron steps (1) - (4) in alkaline conditions, where * represents the active sites, and OOH^*, O^* and OH^* are adsorbed intermediates.

$$* + O_2 + H^+ + e^- \rightarrow OOH^* \quad \text{..... (1)}$$

$$OOH^* + H^+ + e^- \rightarrow O^* + H_2O \quad \text{..... (2)}$$

$$O^* + H^+ + e^- \rightarrow OH^* \quad \text{(3)}$$

$$OH^* + H^+ + e^- \rightarrow H_2O \quad \text{(4)}$$

The adsorption energies (ΔE) of oxygenated intermediates on $Au_{27}Cd_2$ nanostructures were calculated by

$$\Delta E_{OOH^*} = E_{OOH^*} - E_* - (2E_{H2O} - 3/2E_{H2}) \quad \text{(5)}$$

$$\Delta E_{O^*} = E_{O^*} - E_* - (E_{H2O} - E_{H2}) \quad \text{(6)}$$

$$\Delta E_{OH^*} = E_{OH^*} - E_* - (E_{H2O} - 1/2E_{H2}) \quad \text{(7)}$$

in which E_*, E_{OOH^*}, E_{O^*} and E_{OH^*} are the electronic energies of a clean surface and surfaces adsorbed with OOH^*, O^* and OH^*, respectively. E_{H2O} and E_{H2} are the calculated DFT energies of H_2O and H_2 molecules in the gas phase using the approaches outlined by Nørskov et al.[11] Then the adsorption free energies (ΔG_{ads}) can be obtained by the zero-point energy (ZPE) and the entropy (TS) corrections in equation (8):

$$\Delta G_{ads} = \Delta E + \Delta ZPE - T\Delta S \quad \text{(8)}$$

Where the ΔZPE and ΔS could be obtained from the calculation of vibrational frequencies for the adsorbed species (only adsorbed species are relaxed, and the catalyst is fixed), T is temperature (298.15 K). The ZPE and TS and DFT energies (E) to the free energies. The change in Gibbs free energy (ΔG) during the chemical reaction can be calculated by

$$\Delta G = \Delta G_{ads} + \Delta G_U + \Delta G_{PH} \quad \text{(9)}$$

in which $\Delta G_U = -neU$, where U is the potential at the electrode, and n is the number of transferred charge, ΔG_{pH} is the correction of the free energy under any pH value calculated by

$$\Delta G_{PH} = -KTln[H^+] = -KTln10 * pH \quad \text{(10)}$$

where the pH value is chosen to be 14 in our DFT calculations. The step with the smallest decrease is the potential-determining step (PDS), and its free energy change is ΔG^{min}. The theoretical overpotential (η) of ORR is given by

$$\eta^{ORR} = 1.23 - \Delta G^{min}/e \quad \text{(11)}$$

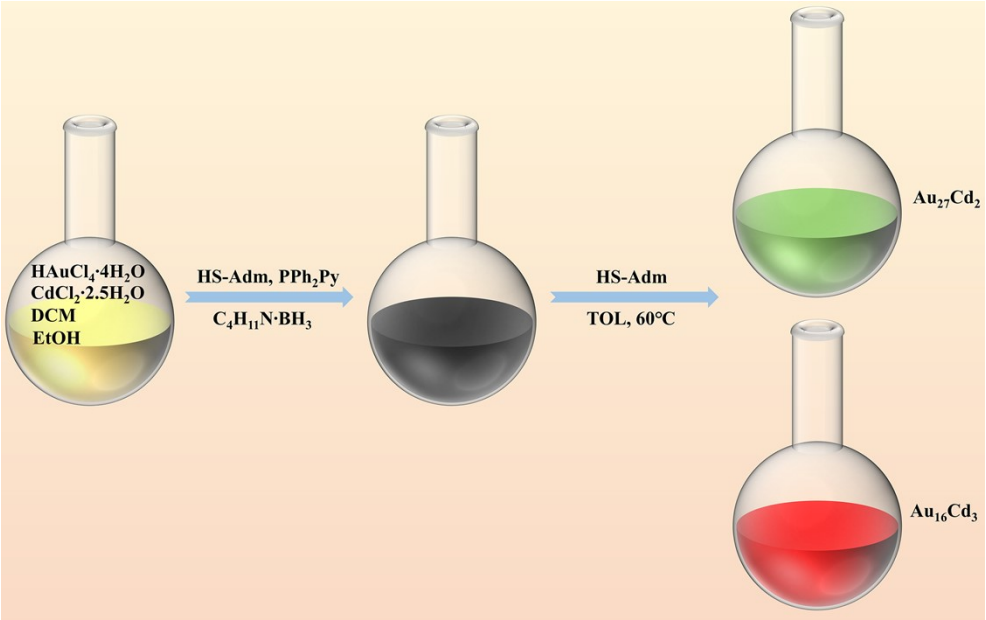

Fig. S1 The synthesis routes of $Au_{27}Cd_2$ and $Au_{16}Cd_3$ clusters.

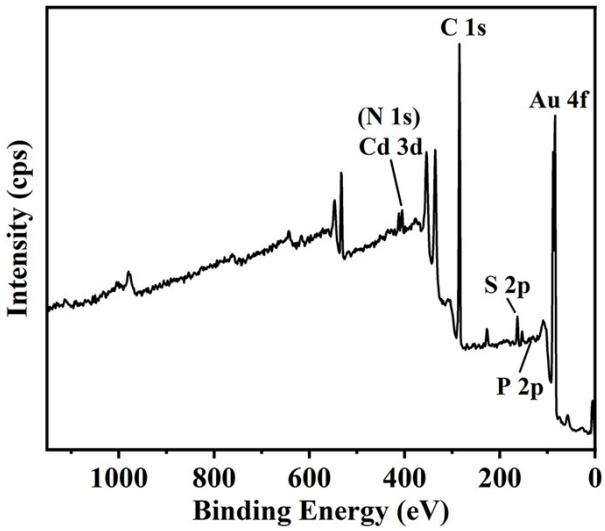

Fig. S2 The XPS spectrum of $Au_{27}Cd_2$.

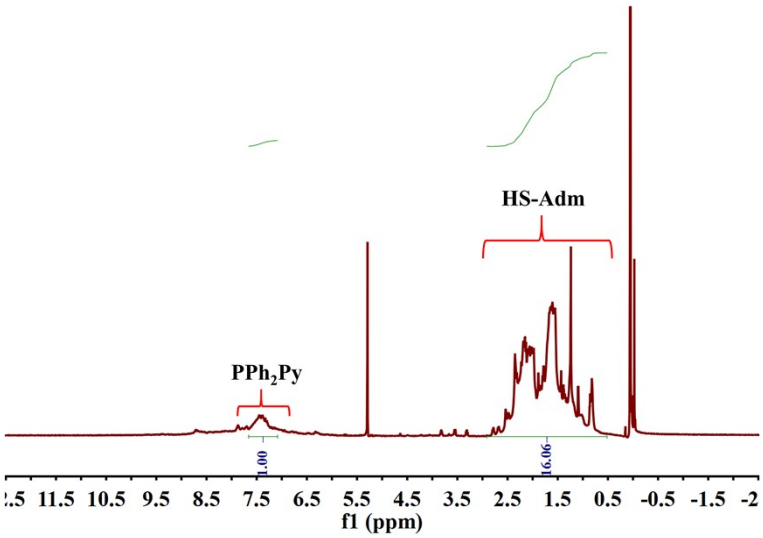

Fig. S3 ^1H NMR spectrum of the $Au_{27}Cd_2$ cluster.

Table S1. Crystal data and structure refinement for $Au_{27}Cd_2$.

CCDC code	2381499
Empirical formula	$C_{177}H_{254}Au_{27}Cd_2S_{16}ClNP$
Formula weight	8518.07
Temperature/K	120.0
Crystal system	monoclinic
Space group	$P2_1/n$
a/Å	17.3748(3)
b/Å	32.3965(4)
c/Å	38.6842(6)
α/°	90
β/°	97.4160(10)
γ/°	90
Volume/Å^3	21592.5(6)
Z	4
ρ_{calc}g/cm^3	2.620
μ/mm^{-1}	36.961
F(000)	15360.0
Crystal size/mm^3	0.08 × 0.1 × 0.08
Radiation	CuKα (λ = 1.54186)
2Θ range for data collection/°	5.888 to 131.996
Index ranges	$-13 \le h \le 20$, $-38 \le k \le 37$, $-38 \le l \le 45$
Reflections collected	87221
Independent reflections	35798 [R_{int} = 0.0825, R_{sigma} = 0.2038]
Data/restraints/parameters	35798/2406/2153
Goodness-of-fit on F^2	0.712
Final R indexes [I>=2σ (I)]	R_1 = 0.0488, wR_2 = 0.0958
Final R indexes [all data]	R_1 = 0.0953, wR_2 = 0.1033
Largest diff. peak/hole / e Å^{-3}	2.48/-1.47

Table S2. EA of the $Au_{27}Cd_2$ cluster.

Empirical formula	C	H	N
$C_{177}H_{254}Au_{27}Cd_2Cl_1N_1P_1S_{16}$	24.95%	3%	0.15%

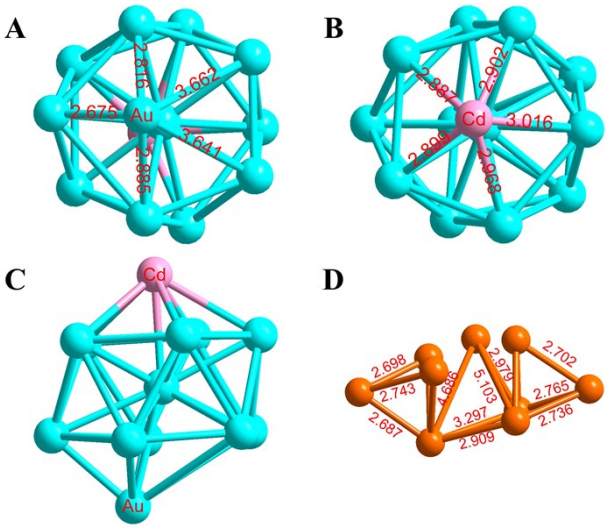

Fig. S4 Core analysis diagram of $Au_{27}Cd_2$. (A) Au-Au bond length in $Au_{12}Cd_1$ core, (B) Au-Cd bond length in $Au_{12}Cd_1$ core, (C) distortion diagram of $Au_{12}Cd_1$, (D) the Au-Au bond lengths in the three tetrahedra.

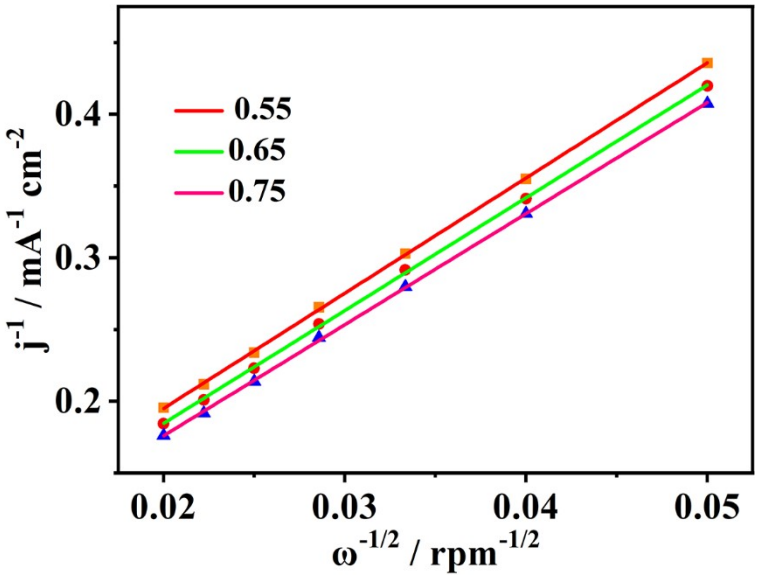

Fig. S5 Koutecky–Levich plots of $Au_{27}Cd_2$ catalysis at different potentials.

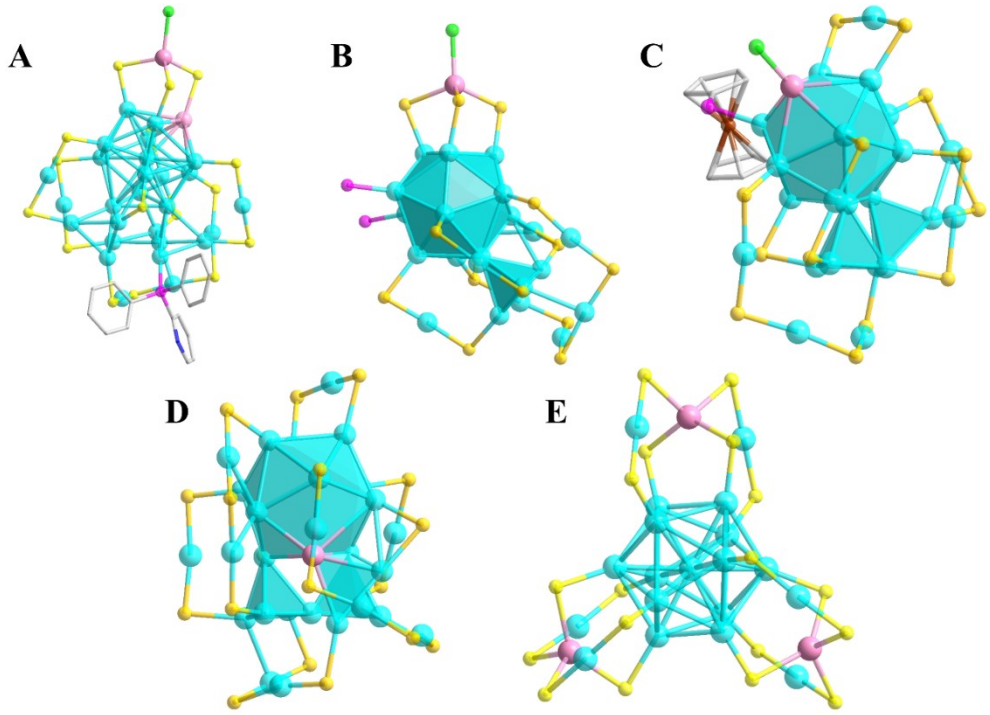

Fig. S6 The Cd distribution in $Au_{27}Cd_2$ (A), $Au_{23}Cd_1$ (B), $Au_{24}Cd_1$ (C), $Au_{30}Cd_1$ (D) and $Au_{19}Cd_3$ (E) (color label: orange = Au, pink = Cd, yellow = S, purple = P, bright green = Cl, blue = N, and parts of C and all H atoms were omitted for clarity).

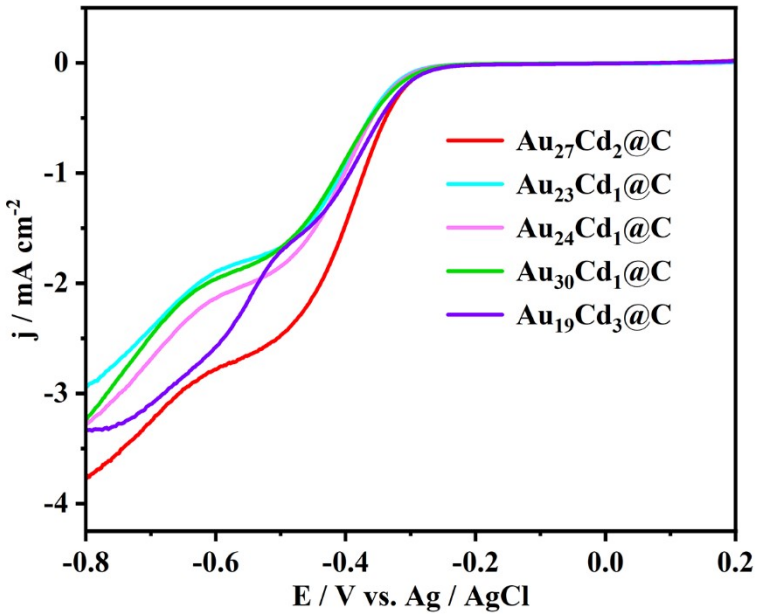

Fig. S7 The LSV curves of the Au-Cd bimetallic catalyst at 1600 rpm.

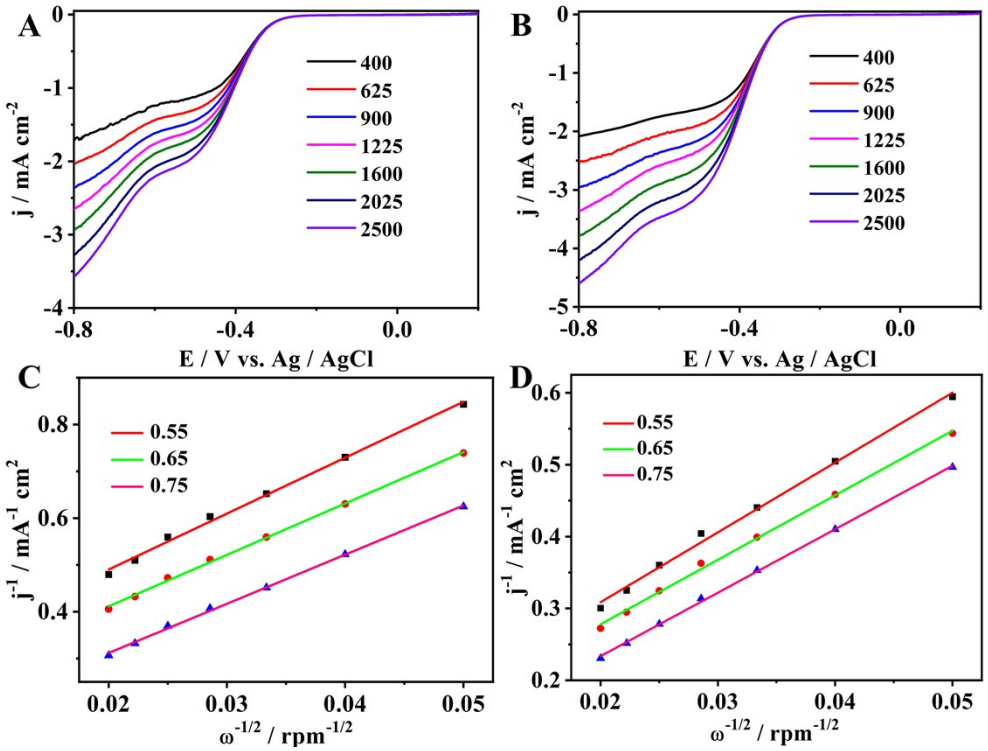

Fig. S8 The ORR LSV curves and Koutecky–Levich plots of $Au_{23}Cd_1$ catalysis before (A, C) and after (B, D) addition of pyridine.

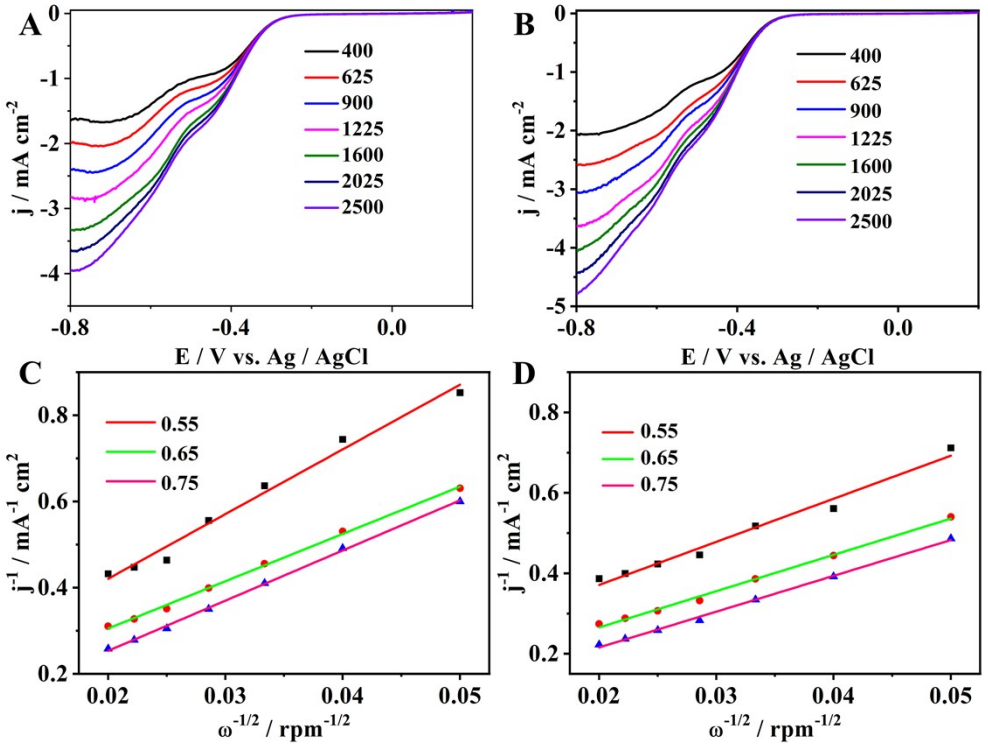

Fig. S9 The ORR LSV curves and Koutecky–Levich plots of $Au_{19}Cd_3$ catalysis before (A, C) and after (B, D) addition of pyridine.

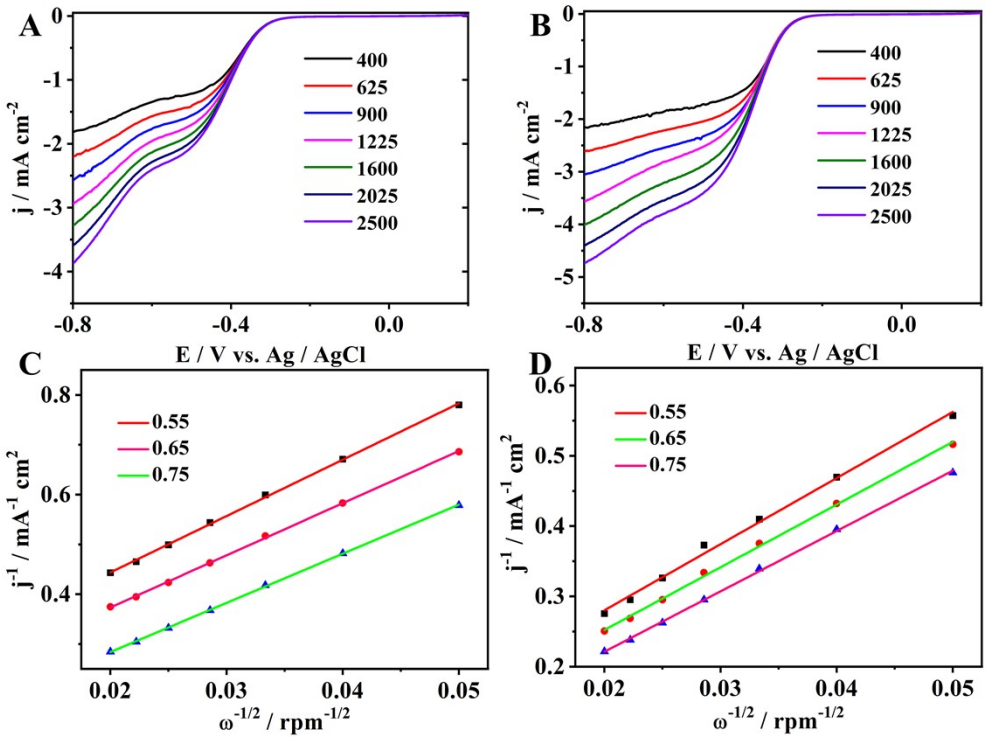

Fig. S10 The ORR LSV curves and Koutecky–Levich plots of $Au_{24}Cd_1$ catalysis before (A, C) and after (B, D) addition of pyridine.

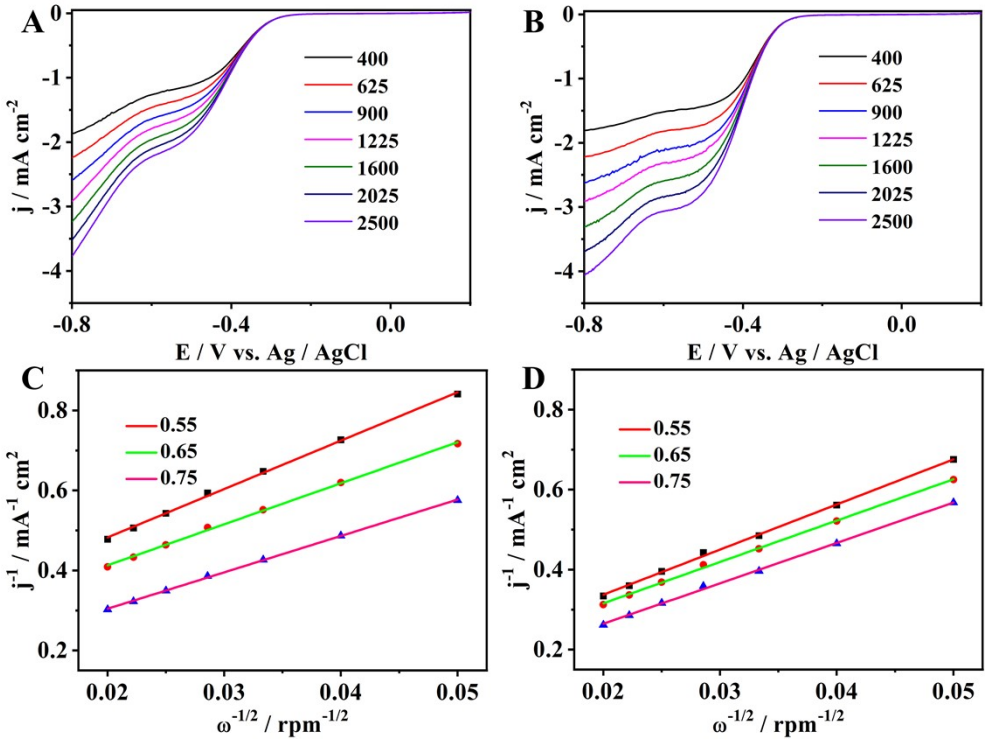

Fig. S11 The ORR LSV curves and Koutecky–Levich plots of $Au_{30}Cd_1$ catalysis before (A, C) and after (B, D) addition of pyridine.

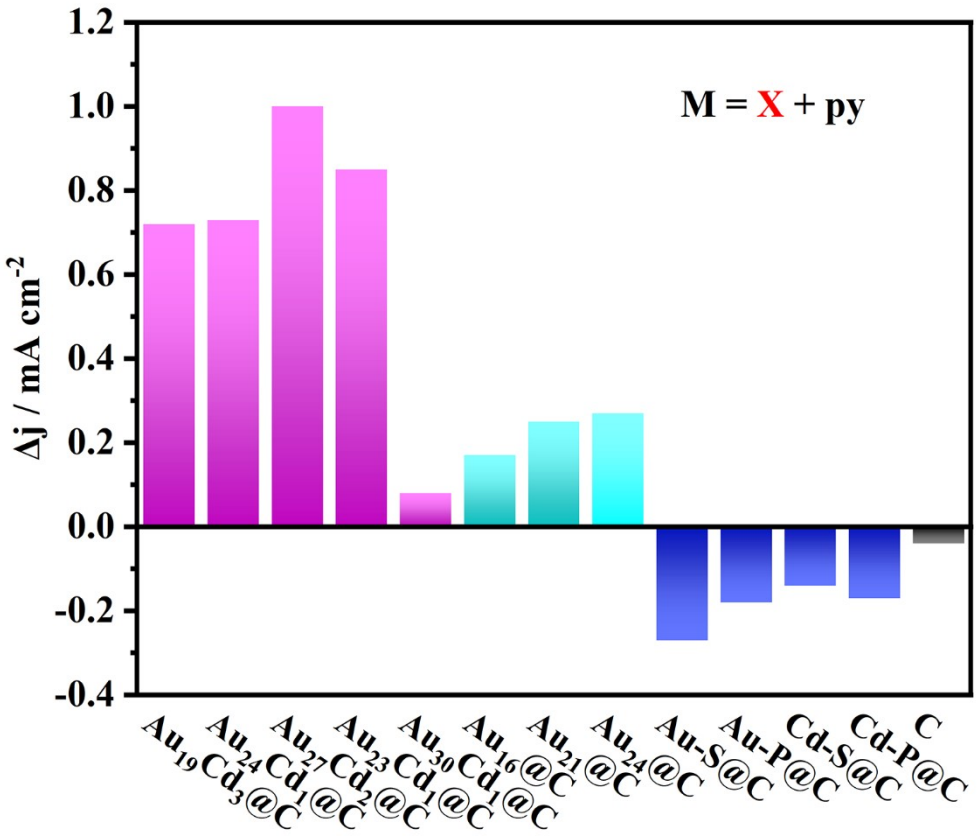

Fig. S12 Comparison of the current densities at -0.8 V of the catalysts before and after the addition of pyridine.

Table S3. Performance comparison and percentage enhancement of all catalysts before and after pyridine addition.

Catalysts	Before adding pyridine ($mA \cdot cm^{-2}$)	After adding pyridine ($mA \cdot cm^{-2}$)	Percentage increase (%)
$Au_{27}Cd_2$@C	3.70	4.70	27.03
$Au_{23}Cd_1$@C	2.93	3.78	28.88
$Au_{24}Cd_1$@C	3.27	4.00	22.32
$Au_{19}Cd_3$@C	3.32	4.04	21.69
$Au_{30}Cd_1$@C	3.23	3.31	2.48
Au_{16}@C	2.48	2.65	6.85
Au_{21}@C	2.60	2.85	9.62
Au_{24}@C	2.63	2.90	10.27
Au-S@C	3.19	2.92	-8.46
Au-P@C	3.00	2.82	-6.00
Cd-S@C	2.88	2.74	-4.86
Cd-P@C	2.93	2.76	-5.80
C	2.45	2.41	-1.63
$Au_{27}Cd_2$@C-NO_3RR	41.78	61.75	47.80
$Au_{27}Cd_2$@C-HER	22.71	43.63	92.12

Table S4. Half-wave potentials of AuCd clusters before and after adding pyridine.

clusters	half-wave potential (V)	
	Before adding pyridine	After adding pyridine
$Au_{27}Cd_2$@C	-0.43	-0.37
$Au_{16}Cd_3$@C	-0.39	-0.39
$Au_{19}Cd_3$@C	-0.50	-0.50
$Au_{23}Cd_1$@C	-0.46	-0.42
$Au_{24}Cd_1$@C	-0.46	-0.40
$Au_{30}Cd_1$@C	-0.46	-0.43

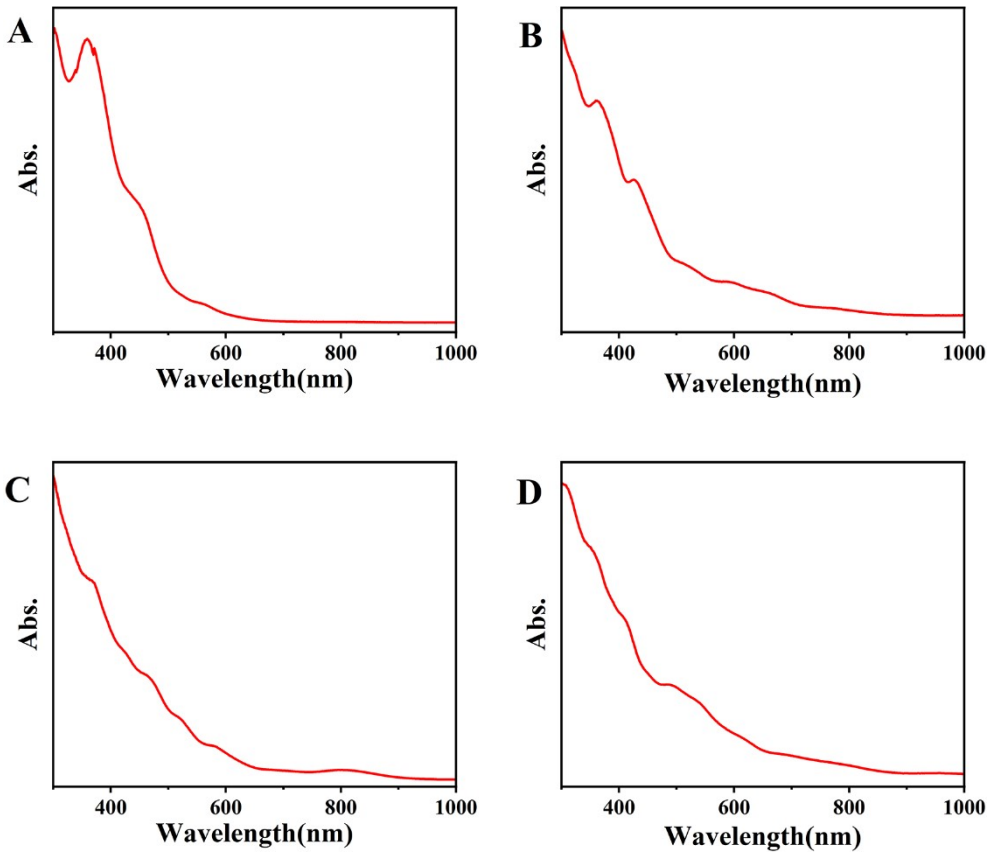

Fig. S13 UV-vis spectra of (A) $Au_{19}Cd_3$, (B) $Au_{23}Cd_1$, (C) $Au_{24}Cd_1$, and (D) $Au_{30}Cd_1$.

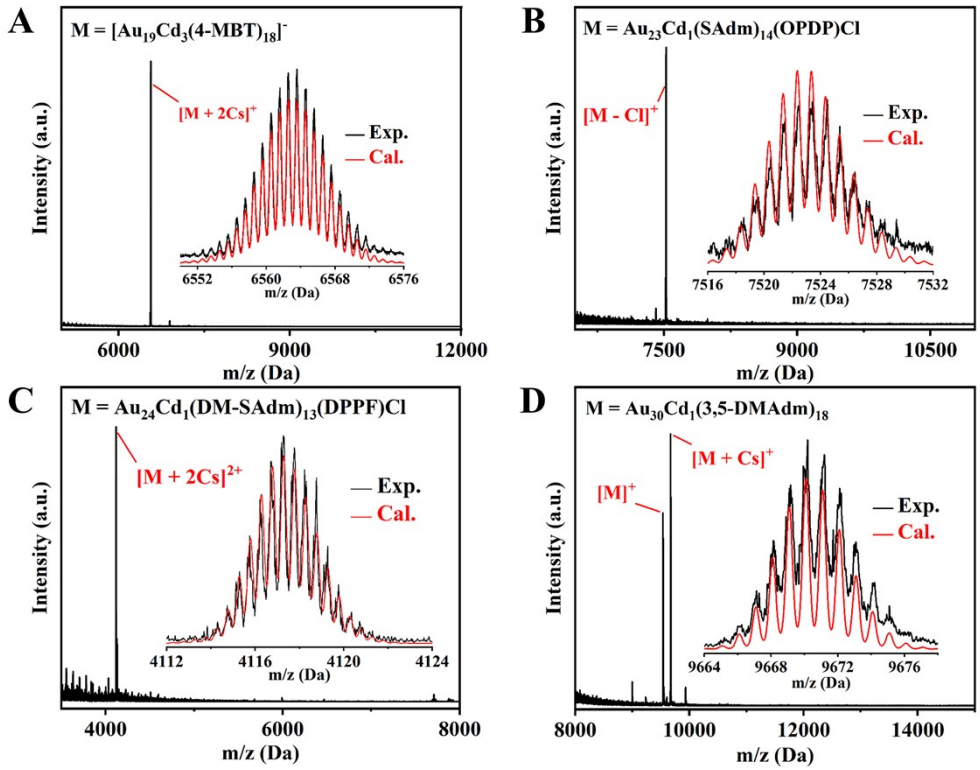

Fig. S14 The ESI-MS spectra of $Au_{19}Cd_3$ (A), $Au_{23}Cd_1$ (B), $Au_{24}Cd_1$ (C), and $Au_{30}Cd_1$ (D).

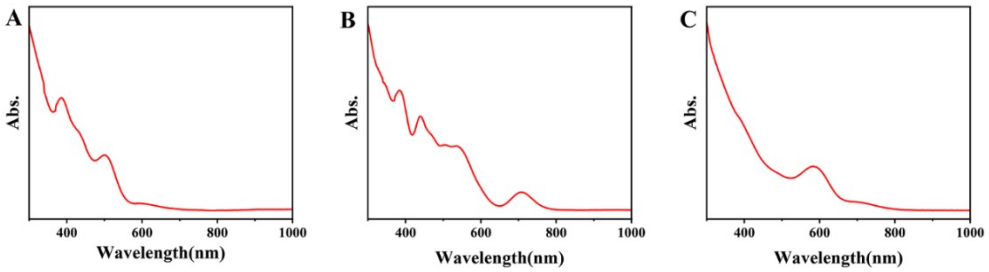

Fig. S15 UV-vis spectra of (A) Au_{16}(S-Adm)$_{12}$, (B) Au_{21}(S-Adm)$_{15}$, and (C) Au_{24}(S-Adm)$_{16}$.

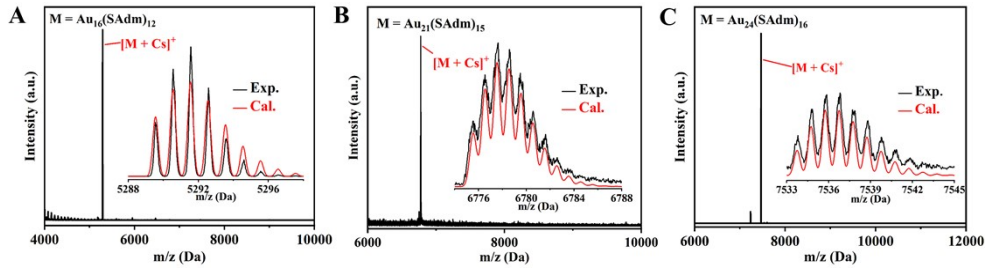

Fig. S16 The ESI-MS spectra of Au_{16} (A), Au_{21} (B), and Au_{24} (C).

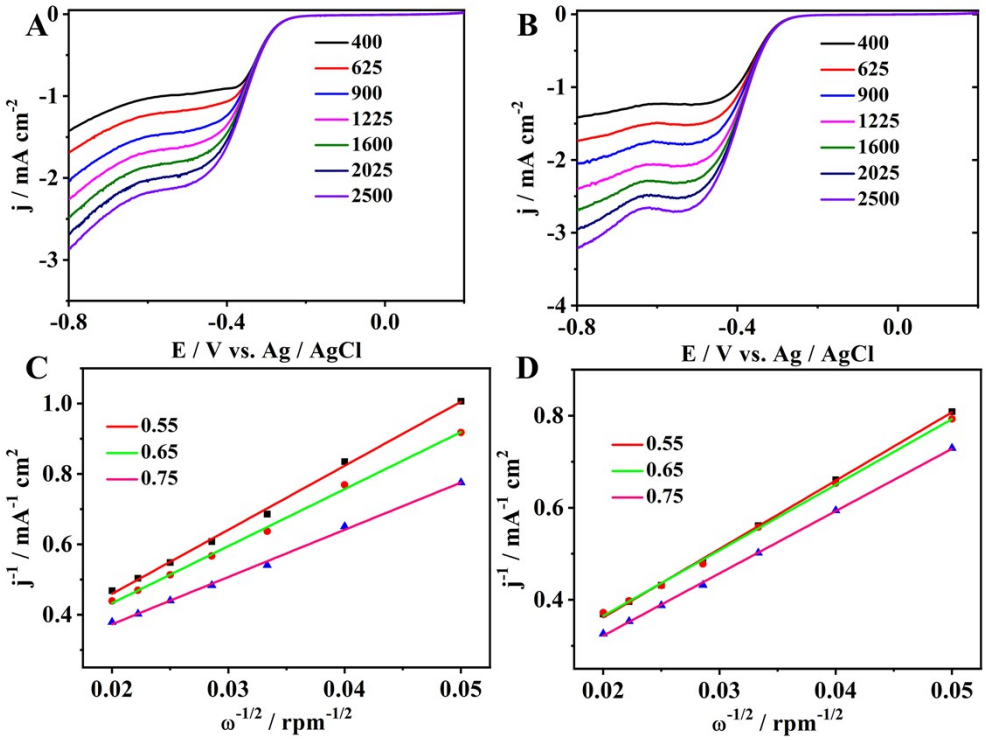

Fig. S17 The ORR LSV curves and Koutecky–Levich plots of Au_{16} catalysis before (A, C) and after (B, D) addition of pyridine.

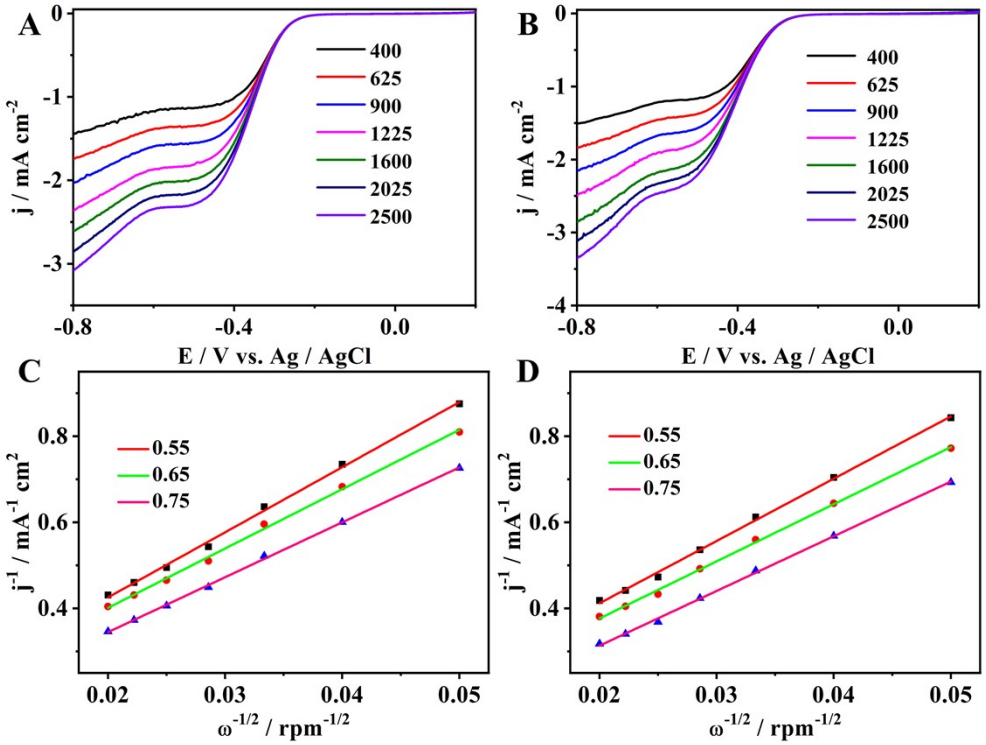

Fig. S18 The ORR LSV curves and Koutecky–Levich plots of Au_{21} catalysis before (A, C) and after (B, D) addition of pyridine.

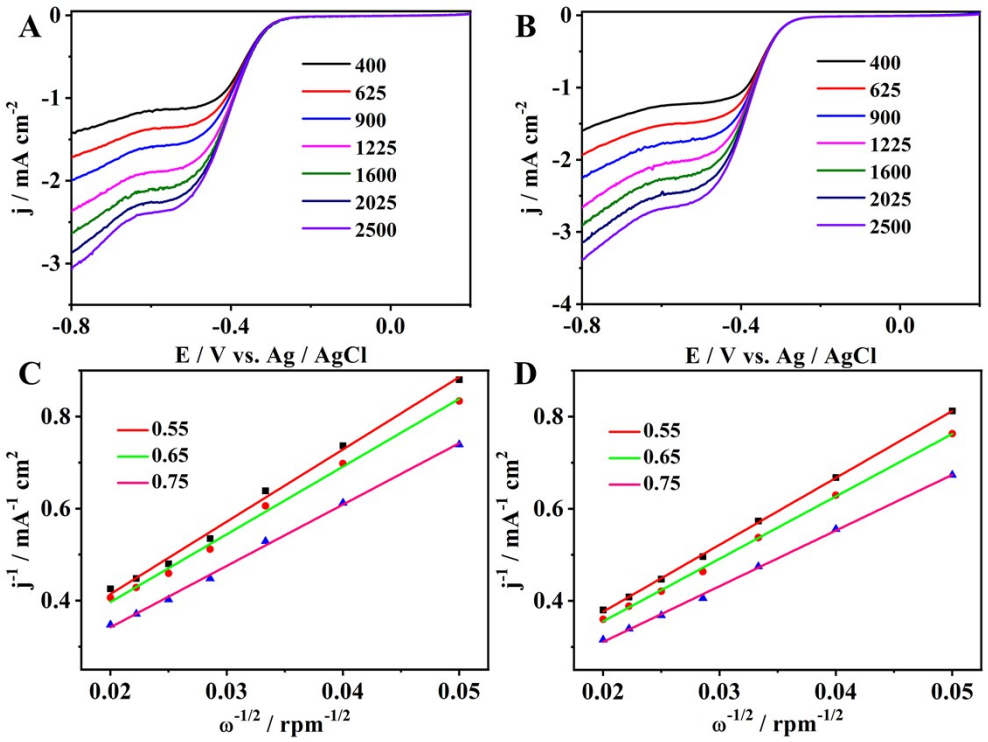

Fig. S19 The ORR LSV curves and Koutecky–Levich plots of Au_{24} catalysis before (A, C) and after (B, D) addition of pyridine.

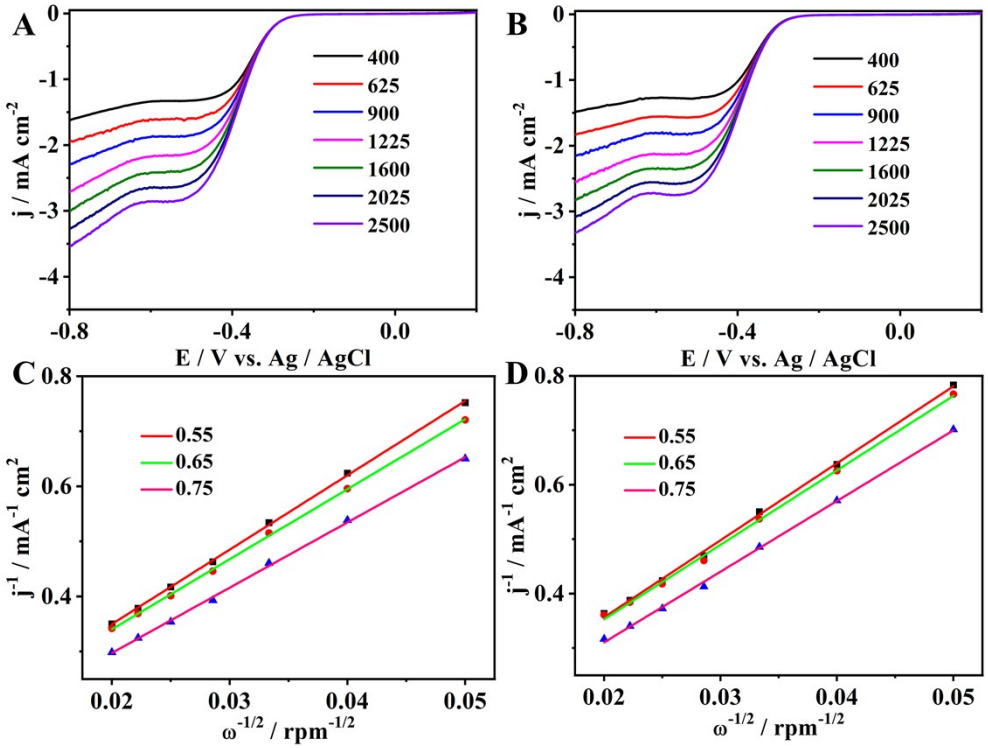

Fig. S20 The ORR LSV curves and Koutecky–Levich plots of Au-P complex catalysis before (A, C) and after (B, D) addition of pyridine.

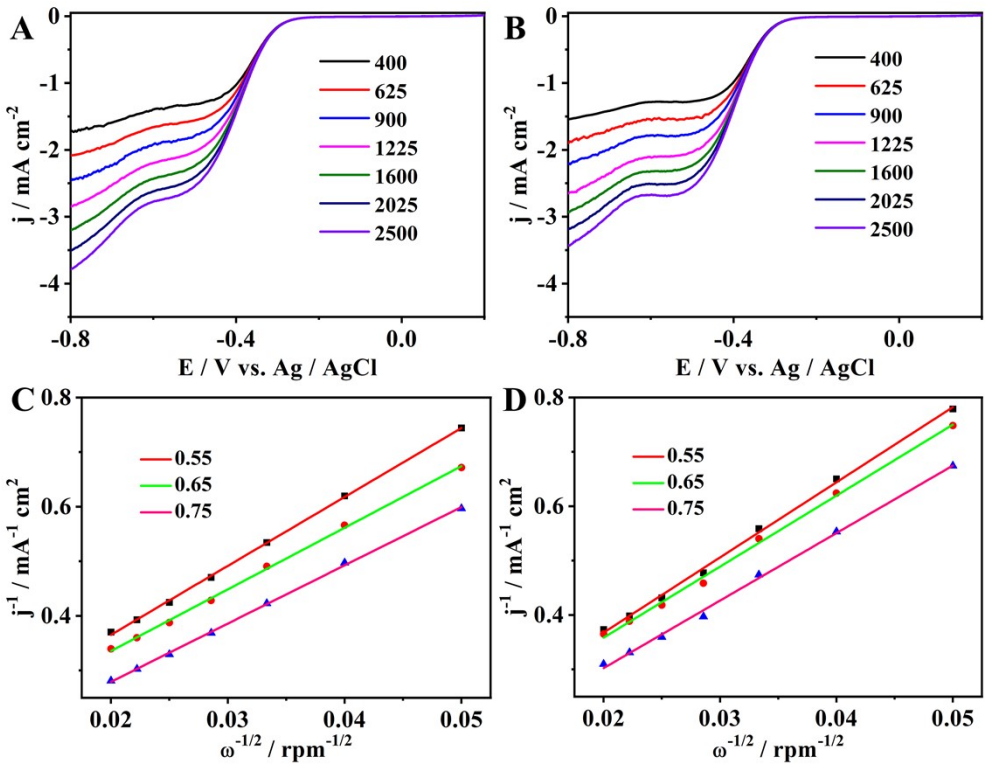

Fig. S21 The ORR LSV curves and Koutecky–Levich plots of Au-S complex catalysis before (A, C) and after (B, D) addition of pyridine.

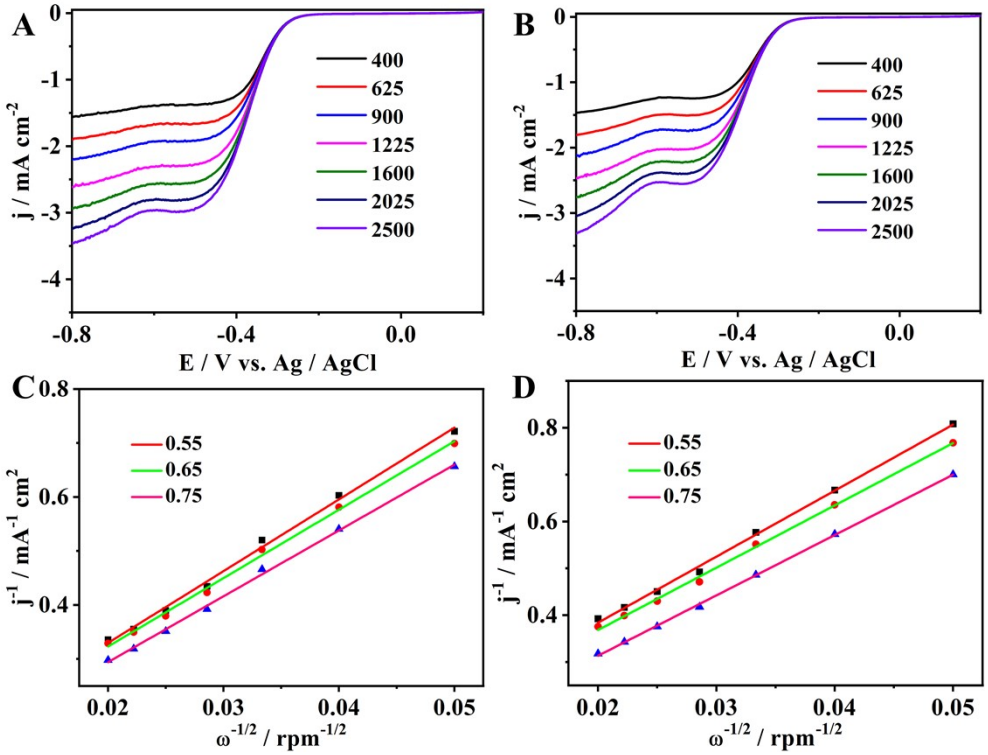

Fig. S22 The ORR LSV curves and Koutecky–Levich plots of Cd-P complex catalysis before (A, C) and after (B, D) addition of pyridine.

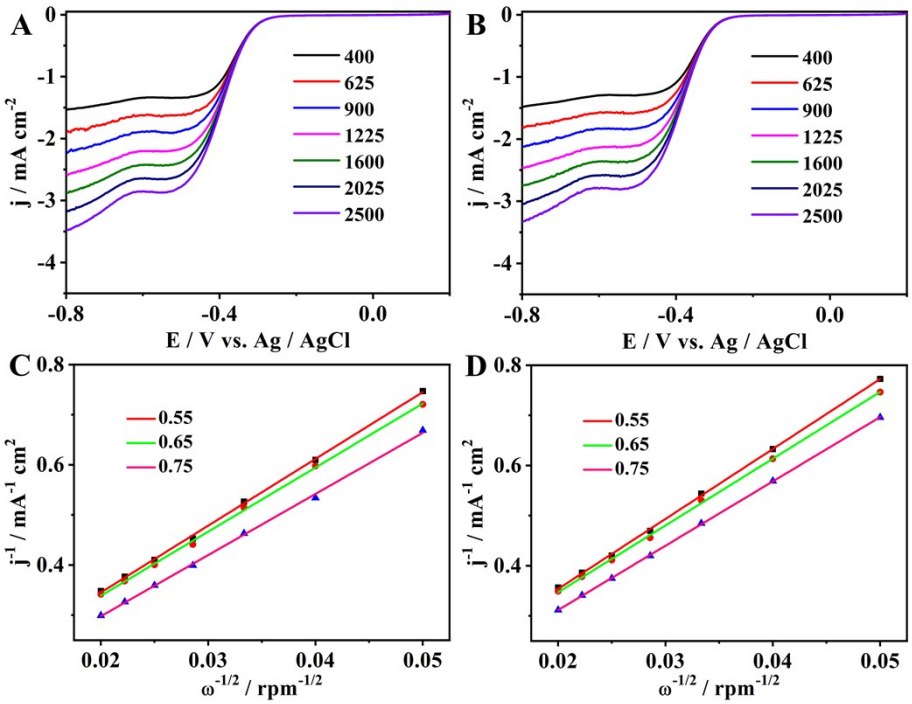

Fig. S23 The ORR LSV curves and Koutecky–Levich plots of Cd-S complex catalysis before (A, C) and after (B, D) addition of pyridine.

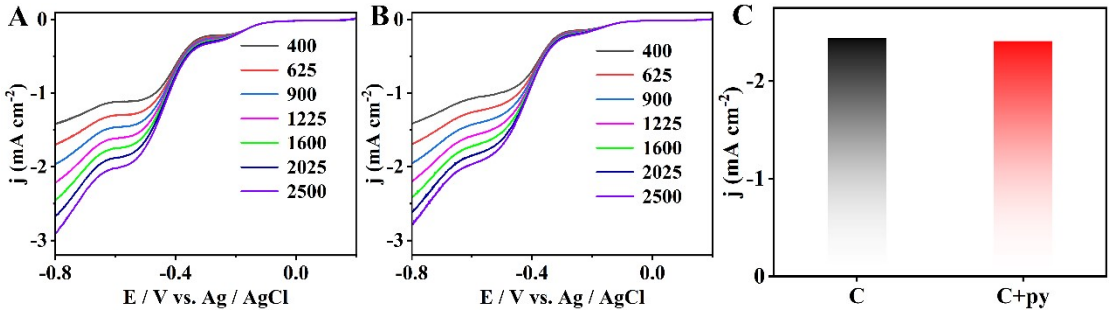

Fig. S24 The ORR LSV curves of activated carbon before and after the addition of pyridine.

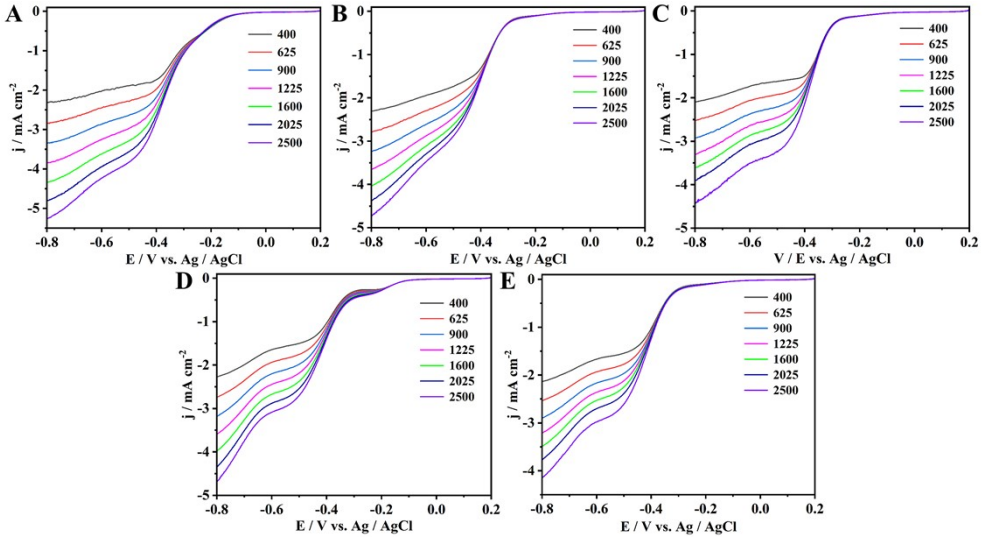

Fig. S25 The ORR LSV curves of $Au_{27}Cd_2$@C after adding (A) Piperidine, (B) Pyrrolidine, (C) Piperazine, (D) Diethylamine, and (E) Triethylamine.

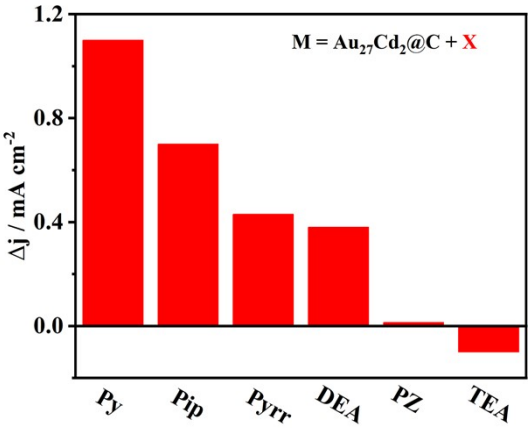

Fig. S26 Bar chart of current density differences after adding different additives. (Py = Pyridine, Pip = Piperidine, Pyrr = Pyrrolidine, DEA = Diethylamine, PZ = Piperazine and TEA = Triethylamine).

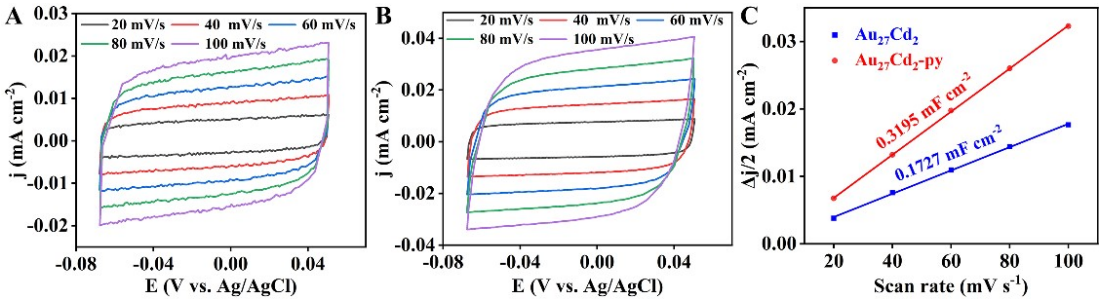

Fig. S27 CV curves of (A) $Au_{27}Cd_2$ and (B) $Au_{27}Cd_2$-py at different scan rates (20-100 mV s^{-1}) and (C) double-layer capacitance (C_{dl}) of $Au_{27}Cd_2$ and $Au_{27}Cd_2$-py measured in 0.5 M K_2SO_4 solution with 0.1 M NO_3^-, where $\Delta j/2 = (j_a - j_c)/2$ (j_a and j_c denote the anode and cathode current density).

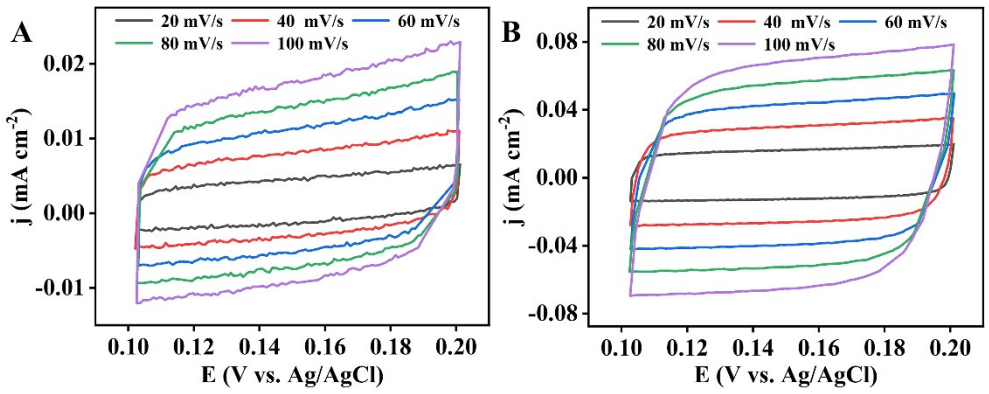

Fig. S28 CV curves of (A) $Au_{27}Cd_2$@C and (B) $Au_{27}Cd_2$@C-py at different scan rates (20-100 mV s^{-1}).

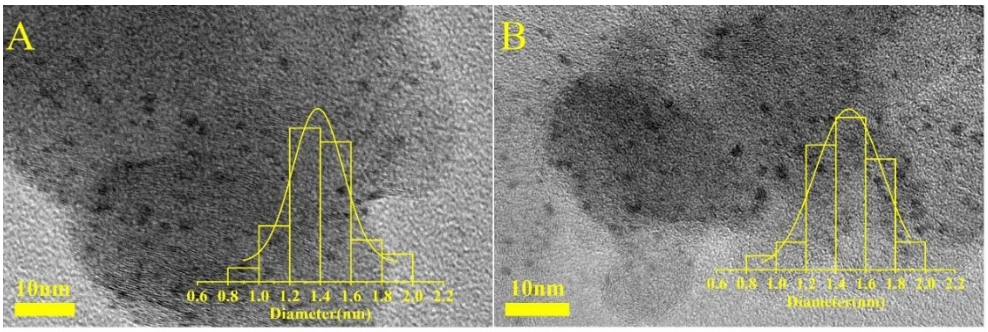

Fig. S29 TEM and size distribution of $Au_{27}Cd_2$@C before (A) and after (B) tests.

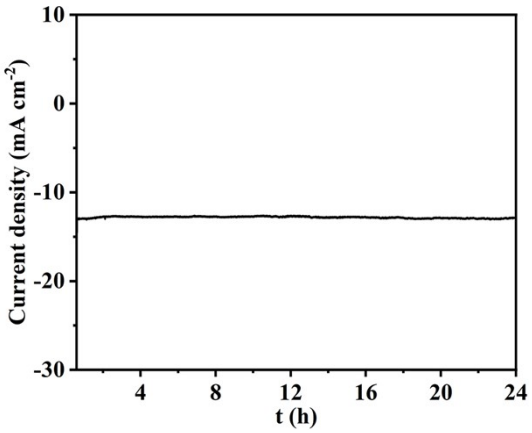

Fig. S30 The Current-Time (IT) curve of $Au_{27}Cd_2$@C at -1.4V for 24 hours.

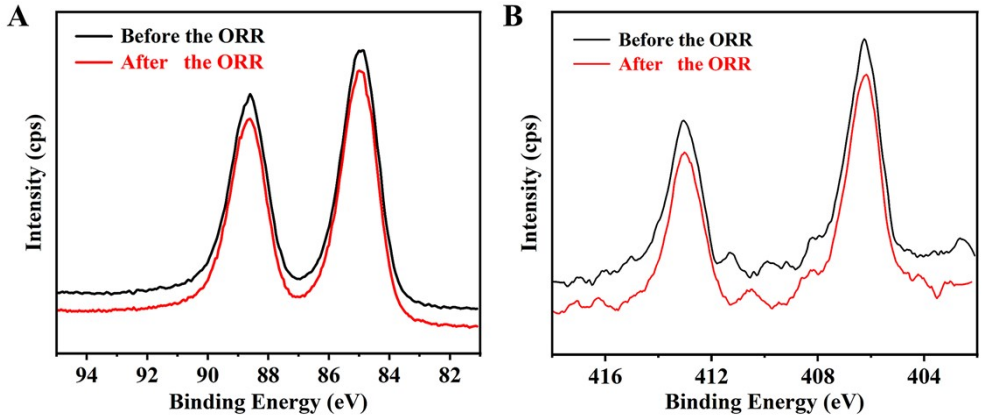

Fig. S31 (A) Au 4f and (B) Cd 3d binding energy of $Au_{27}Cd_2$@C in XPS spectra, before and after the ORR reaction.

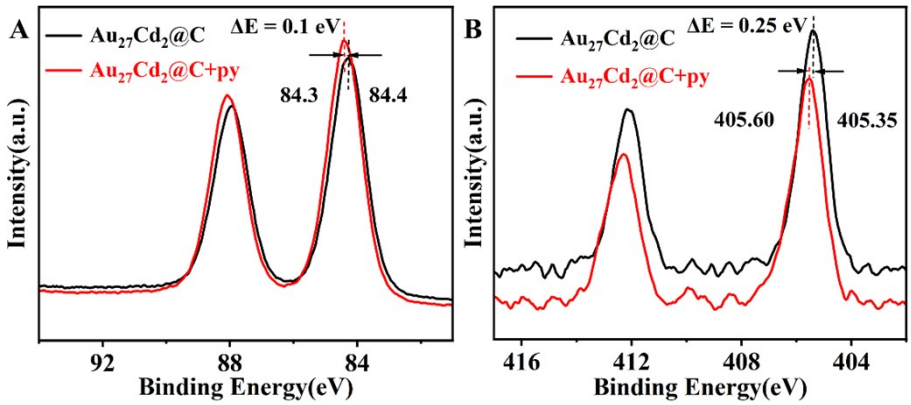

Fig. S32 Changes of $Au_{27}Cd_2$@C XPS absorption peak before and after the addition of pyridine. (A) Au 4f and (B) Cd 3d.

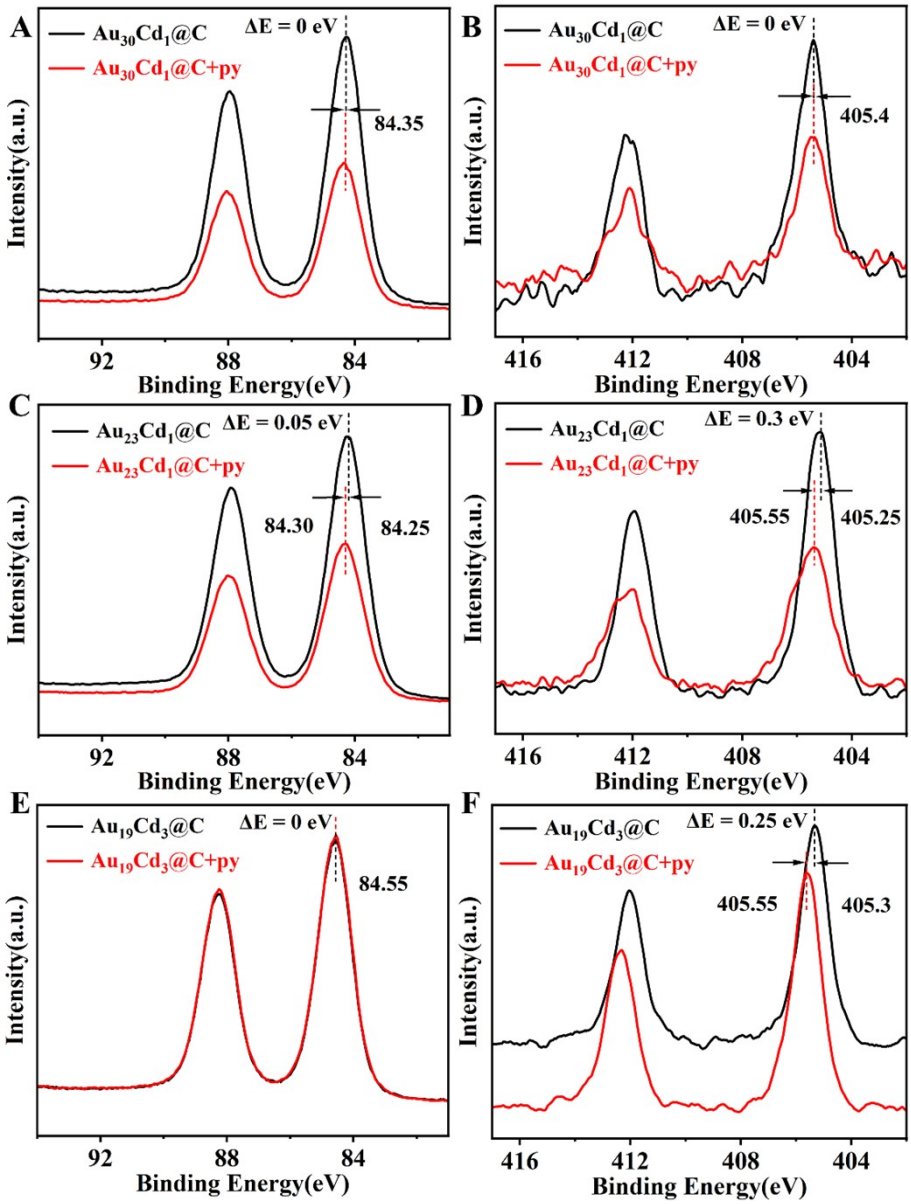

Fig. S33 Changes of $Au_{30}Cd_1$@C, $Au_{23}Cd_1$@C, and $Au_{19}Cd_3$@C XPS absorption peak before and after the addition of pyridine. (A) Au 4f and (B) Cd 3d of $Au_{30}Cd_1$, (C) Au 4f and (D) Cd 3d of $Au_{23}Cd_1$, (E) Au 4f and (F) Cd 3d of $Au_{19}Cd_3$.

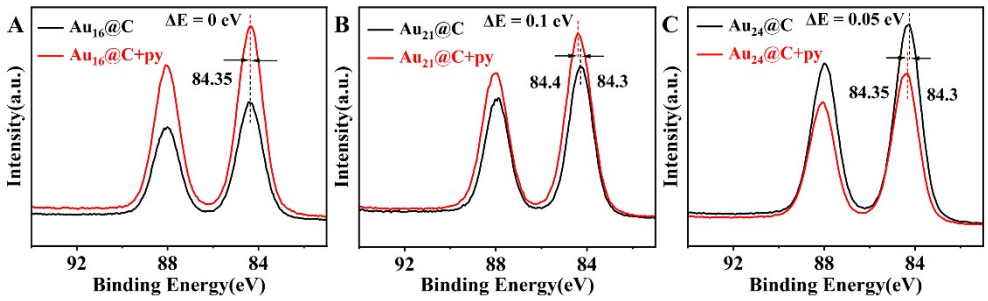

Fig. S34 Changes of Au 4f XPS absorption peak in (A) Au_{16}@C, (B) Au_{21}@C, and (C) Au_{24}@C before and after the addition of pyridine.

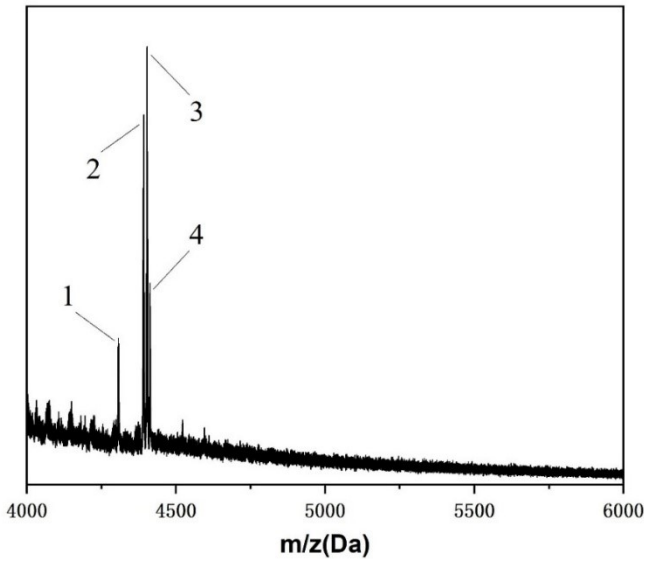

Fig. S35 The total ESI-MS spectrum of $Au_{27}Cd_2$ after the addition of pyridine. Signal peaks 1-4 are assigned to $[Au_{27}Cd_2(S\text{-}Adm)_{15}(PPh_2Py)Cl+2Cs]^{2+}$, $[Au_{27}Cd_2(S\text{-}Adm)_{16}(PPh_2Py)Cl+2Cs]^{2+}$, $[Au_{27}Cd_2(S\text{-}Adm)_{16}(PPh_2Py)(CH_3COO^-)+2Cs]^{2+}$, $[Au_{27}Cd_2(S\text{-}Adm)_{16}(PPh_2Py)(Py)+2Cs]^{2+}$.

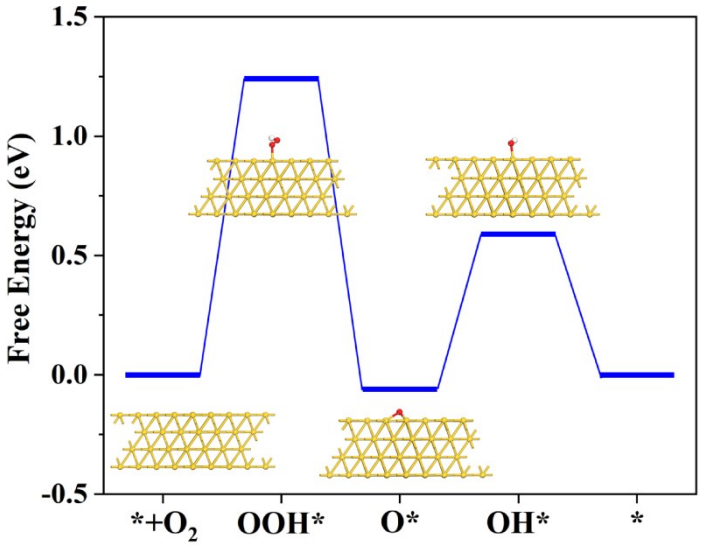

Fig. S36 Free energy diagrams of ORR at Au(111) surfaces (U^0 = 1.23 V).

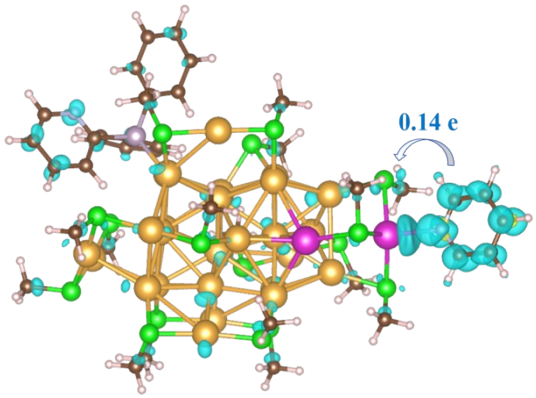

Fig. S37 The charge differential density and Bader charge analysis of $Au_{27}Cd_2$ nanostructures with pyridine modification.

Table S5. Calculated Gibbs free energies (G_{ads}*) for OOH*, O*, and OH*, including zero-point energy (ZPE) and entropy (TΔS) corrections.

		E	TΔS	ZPE	G_{ads}*
$Au_{27}Cd_2$	*	-702.70	/	/	/
	OH*	-712.51	0.36	0.64	1.35
	O*	-708.64	0.08	0.14	1.55
	OOH*	-716.77	0.37	0.87	4.74
$Au_{27}Cd_2$-py	*	-776.03	/	/	/
	OH*	-786.01	0.20	0.70	1.41
	O*	-780.70	0.09	0.13	2.80
	OOH*	-790.31	0.31	0.85	4.57
H_2O		-14.22	0.67	0.56	/
H_2		-6.76	0.41	0.27	/

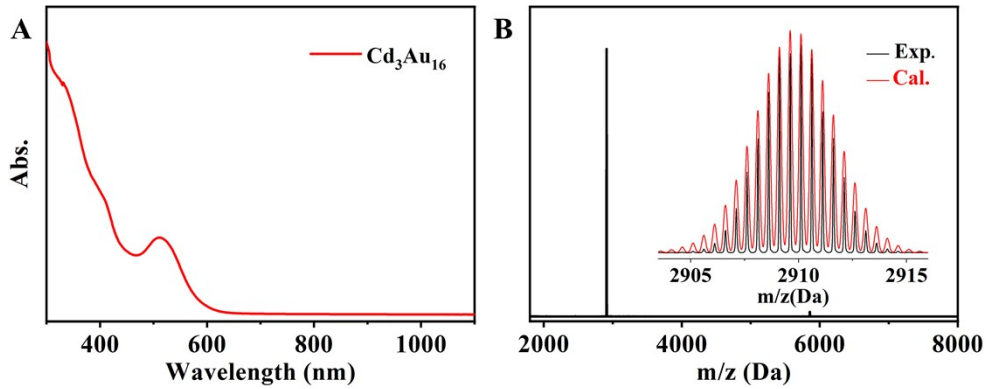

Fig. S38 (A) UV-vis spectrum and (B) ESI-MS of $Au_{16}Cd_3$.

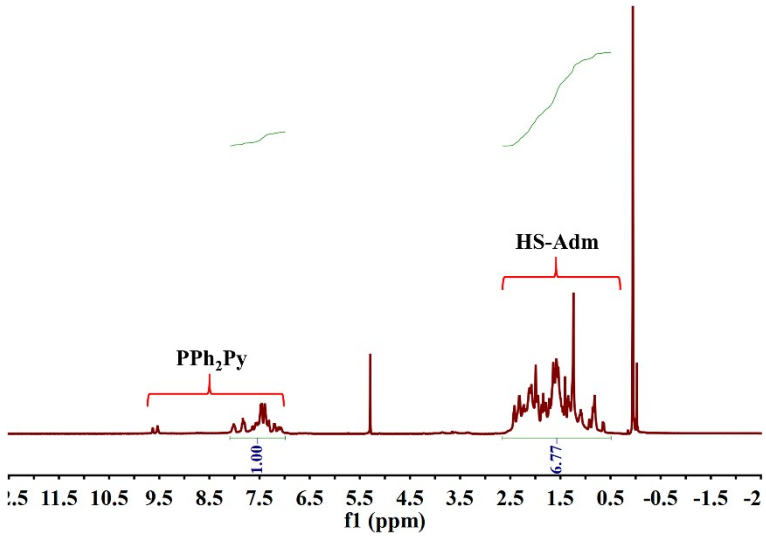

Fig. S39 ^{1}H NMR spectrum of the $Au_{16}Cd_3$ cluster.

Table S6. CHN EA of the $Au_{16}Cd_3$ cluster.

Empirical formula	C	H	N
$C_{141}H_{177}Au_{16}Cd_3Cl_3N_3P_3S_9$	28.7%	3%	0.7%

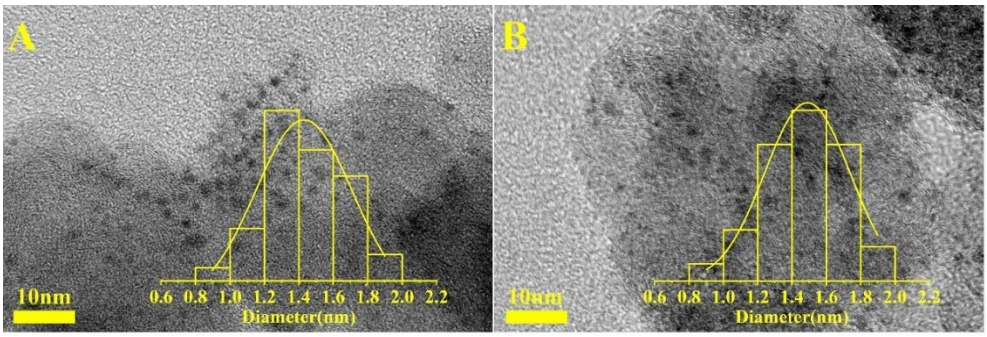

Fig. S40 TEM and size distribution of $Au_{16}Cd_3$@C before (A) and after (B) tests.

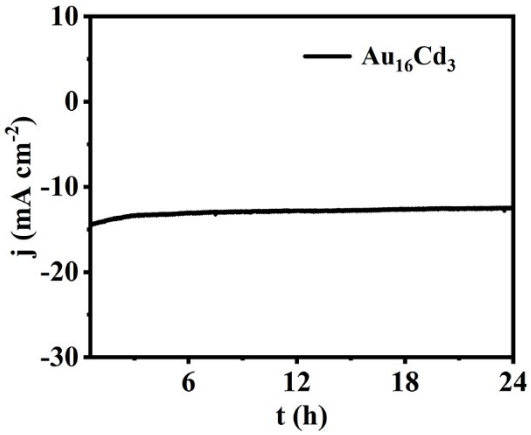

Fig. S41. The IT curves of $Au_{16}Cd_3$@C (F) at -1.4V for 24 hours.

Table S7. Crystal data and structure refinement for $Au_{16}Cd_3$.

CCDC code	2381500
Empirical formula	$C_{141}H_{177}Au_{16}Cd_3Cl_3N_3P_3S_9$
Formula weight	5890.31
Temperature/K	120.0
Crystal system	triclinic
Space group	P-1
a/Å	16.8145(4)
b/Å	17.0639(4)
c/Å	31.7354(8)
α/°	82.183(2)
β/°	84.464(2)
γ/°	63.191(2)
Volume/Å^3	8045.0(4)
Z	2
ρ_{calc}g/cm^3	2.432
μ/mm^{-1}	31.903
F(000)	5384.0
Crystal size/mm^3	0.1 × 0.07 × 0.05
Radiation	CuKα (λ = 1.54186)
2Θ range for data collection/°	6.436 to 132
Index ranges	$-19 \le h \le 11$, $-20 \le k \le 16$, $-37 \le l \le 32$
Reflections collected	59840
Independent reflections	26940 [R_{int} = 0.0694, R_{sigma} = 0.1123]
Data/restraints/parameters	26940/1152/1603
Goodness-of-fit on F^2	0.939
Final R indexes [I>=2σ (I)]	R_1 = 0.0729, wR_2 = 0.1781
Final R indexes [all data]	R_1 = 0.1010, wR_2 = 0.1914
Largest diff. peak/hole / e Å^{-3}	5.64/-5.17

Supporting references

1. C. Yao, C. Q. Xu, I. H. Park, M. Zhao, Z. Zhu, J. Li, X. Hai, H. Fang, Y. Zhang, G. Macam, J. Teng, L. Li, Q. H. Xu, F. C. Chuang, J. Lu, C. Su, J. Li and J. Lu, *Angew. Chem. Int. Ed.*, 2020, **59**, 8270-8276.
2. Y. Tan, Y. Lv, L. Xu, Q. Li, J. Chai, S. Yang, H. Yu and M. Zhu, *J. Am. Chem. Soc.*, 2023, **145**, 4238–4245.
3. S. Yang, S. Chen, L. Xiong, C. Liu, H. Yu, S. Wang, N. L. Rosi, Y. Pei and M. Zhu, *J. Am. Chem. Soc.*, 2018, **140**, 10988–10994.
4. S. Chen, L. Xiong, S. Wang, Z. Ma, S. Jin, H. Sheng, Y. Pei and M. Zhu, *J. Am. Chem. Soc.*, 2016, **138**, 10754–10757.
5. D. Crasto, G. Barcaro, M. Stener, L. Sementa, A. Fortunelli and A. Dass, *J. Am. Chem. Soc.*, 2014, **136**, 14933–14940.
6. G. Kresse and J. Hafner, *Phys. Rev. B* 1993, **48**, 13115−13118.
7. P. E. Blöchl, *Phys. Rev. B* 1994, **50**, 17953-17979.
8. J. P. Perdew, K. Burke and M. Ernzerhof, *Phys. Rev. Lett.* 1996, **77**, 3865−3868.
9. Grimme, *J. Comput. Chem.* 2006, **27**, 1787−1799.
10. K. Mathew, R. Sundararaman, K. Letchworth-Weaver, T. A. Arias and R. G. Hennig, *J. Chem. Phys.* 2014, **140**, 84–106.
11. I. C. Man, H. Y. Su, F. Calle-Vallejo, H. A. Hansen, J. I. Martínez, N. G. Inoglu, J. Kitchin, T. F. Jaramillo, J. K. Nørskov and J. Rossmeisl, *ChemCatChem* 2011, **3**, 1159–1165.